Solar pyrolysis of algae in molten salt for capacitive carbon preparation

Jun Li, Jing Peng, Kuo Zeng, Dian Zhong, Kang Xu, Vasilevich Sergey Vladimirovich, Ange Nzihou, Haiping Yang, Hanping Chen

Solar pyrolysis of algae in molten salt for capacitive carbon preparation

Jun Li [a], Jing Peng [b], Kuo Zeng [a,*], Dian Zhong [a], Kang Xu [b], Vasilevich Sergey Vladimirovich [c], Ange Nzihou [d], Haiping Yang [a], Hanping Chen [a]

[a] State Key Laboratory of Coal Combustion, Huazhong University of Science and Technology, 1037 Luoyu Road, Wuhan, Hubei, 430074, PR China
[b] China-EU Institute for Clean and Renewable Energy, Huazhong University of Science and Technology, Wuhan, 430074, China
[c] Institute of Energy, National Academy of Sciences of Belarus, Akademicheskaya Str., 220072, Minsk, Belarus
[d] Université de Toulouse, Mines Albi, UMR CNRS 5302, Centre RAPSODEE, Campus Jarlard, F-81013, Albi, cedex 09, France

Pyrolysis of algae in molten carbonates driven by concentrated solar energy is proposed as an economical and environmentally friendly method to obtain capacitive carbon for supercapacitors. The effects of molten carbonates on pyrolysis process and electrochemical performance at different temperatures (800, 850 and 900 °C) are investigated. Na_2CO_3–K_2CO_3 leads to a relatively high carbon yield and superior microstructure at around 900 °C compared with other molten salts, which is beneficial for capacitive carbon production. The as-prepared carbon possesses a high specific surface area of 2009.26 m^2/g and a hierarchical porous structure mainly consisting of micropores and mesopores. Moreover, it contains abundant oxygen- and nitrogen-containing functional groups, such as C═O, –OH, pyrrolic–N and quaternary–N. These features play an important multiple synergy for the preparation of desirable capacitive carbon, which has a high specific capacitance of 230.2 F/g at 0.25 A/g and a capacitance retention of 75.54% at 2 A/g. This work provides a green and promising approach for the production of heteroatom-doped capacitive carbon with superior porosity and specific surface area.

1. Introduction

Clean sustainable energy and energy storage devices are urgently needed to tackle the deterioration of environmental pollution and global energy crisis. Supercapacitors (SCs) are considered as one of the most promising energy storage devices owing to their high-power density, long cycle life and ultra-fast charge-discharge rate (Dong et al., 2016). Among SCs, the electric double layer capacitors (EDLCs) have wider applications because of their higher power density and cycle stability compared to pseudo-capacitors (Lu et al., 2016a,b,c). For EDLCs appli-cations, carbon materials, especially activated carbons (ACs) derived from biomass, are the ideal candidates for electrode materials by virtue of low cost, environmentally friendly, and tunable specific surface area (SSA) and porosity (Liu et al., 2023; Mao et al., 2020).

Chemical activation a one-step process operated at temperatures ranging from 400 to 900 °C using activators such as KOH, $ZnCl_2$ and KNO_3 for ACs production (Premarathna et al., 2019). It is characterized by short activation time, low energy requirement and admirable porosity and surface area (Naji and Tye, 2022). However, these most frequently applied activators face serious and inevitable problems such as intensive corrosivity (KOH), toxicity ($ZnCl_2$) and thermal instability (KNO_3) in practical application (Gao et al., 2021). It is necessary to look for an activator with good stability and mild properties, while ensuring good activation effects to produce ACs.

On the other hand, the solar pyrolysis of biomass for ACs production has gained attention due to the sustainable and renewable nature of biomass and solar energy. Wang and Lobato-Peralta et al. successfully produced carbon materials suitable for supercapacitors from pinewood and Agave Angustifolia leaves (Lobato-Peralta et al., 2020, 2022; Wang et al., 2020a,b). Moreover, Giwa et al. reported that solar pyrolysis was more economically viable and environmentally friendly than the con-ventional pyrolysis for carbon materials production, with a 33-day shorter payback time, 0.48% higher return on investment, and 62% reduction in CO_2 emissions (Giwa et al., 2019). However, carbon pro-duced from solar pyrolysis still suffers from inhomogeneity caused by the intermittency of solar energy (Zuo et al., 2023) or the directionality of concentrated solar energy (Zhong et al., 2023).

Molten carbonates can be used to address the above challenges faced by activators and carbon materials (Zeng et al., 2020). Firstly, carbonate is a middle alkaline activator with good stability and mild properties.

Secondly, molten carbonates, as a fluidic heat storage medium, can increase the contact area between salt molecules and carbon matrix through diffusion and infiltration, while providing good heat transfer to produce homogeneous ACs (Nzihou et al., 2013; Wei et al., 2020). Moreover, molten salt can also be used as a soft template to form porous carbon structure (Zeng et al., 2018). Therefore, molten carbonates coupled with solar pyrolysis for ACs production from biomass is a promising industrial process.

Currently, several researchers have successfully obtained ACs with considerable capacitance from peanut shell (Yin et al., 2014), bamboo shell (Lu et al., 2016a), tobacco stem (Liu et al., 2021), firewood (Lu et al., 2016b) and boiled coffee beans (Lu et al., 2016c) by using molten carbonates. However, the study of algae as a carbon source has not been found yet. Algae has the advantages of short growth cycle and strong carbon sequestration ability (Tang et al., 2021), and is a promising carbon and nitrogen precursor for ACs production due to its composition of carbohydrate, lipid, dietary fiber and protein. Typically, the incor-poration of heteroatoms (mainly nitrogen and oxygen) can improve the conductivity of ACs and contribute to the pseudo-capacitance (Zou et al., 2020). Algae-derived ACs possess a relatively homogeneous hetero-atoms distribution, avoiding the effect of external doping on the cycling stability of the electrode material (Xie et al., 2020). Most importantly, algae contain little or no lignin, and some species of algae do not even have rigid structural cell walls (Law et al., 2022; Velazquez-Lucio et al., 2018). The special structure of algae is more easily activated into ACs by molten salts, which allows carbonates, a less effective activator (compared to $ZnCl_2$ and KOH), to achieve good activation effect as well. Therefore, solar pyrolysis of algae in molten carbonates for capacitive carbon production must not be rejected.

In this study, pyrolysis experiments of algae (N-rich Spirulina platensis) in molten salt (Na_2CO_3–K_2CO_3 and Li_2CO_3–Na_2CO_3–K_2CO_3) were carried out, and temperature of 800, 850 and 900 °C were chosen to obtain better activation. The pyrolysis process, as well as the physico-chemical properties and electrochemical performance of the as-prepared ACs were analyzed in detail to investigate the potential of solar pyrolysis of algae in molten carbonates for capacitive carbon production.

2. Material and methods

2.1. Materials

The protein-rich Spirulina platensis (SP) was purchased from Qingdao Haixingyuan Biology Technology Co., Ltd, dried at 105 °C for 20 h and then sieved (<30 μm) before experiments. For its ultimate analysis, 47.22 wt% carbon, 10.87 wt% nitrogen, 6.43 wt% hydrogen, 1.97 wt% sulfur and 26.01 wt% oxygen was detected on dry basis.

The alkali carbonates (Na_2CO_3, K_2CO_3 and Li_2CO_3, analytical purity> 99%) were purchased from the Sinopharm Chemical Reagent Co., Ltd (Shanghai, China). The well-mixed Na_2CO_3–K_2CO_3–Li_2CO_3 ternary salts (TS) with a mass ratio of 1:1:1, and the Na_2CO_3–K_2CO_3 binary salts (BS) with a mass ratio of 1.1:1, were prepared using a planetary ball mill (PM 100, Germany) operating at a speed of 400 r/min for 34 min. The melting points of the as-prepared TS and BS are about 397 °C and 709 °C respectively(Yin et al., 2014).

2.2. Experimental methods

The experimental facility for algae pyrolysis with molten carbonates is shown in Fig. S1, which mainly comprises a corundum crucible (80 mm height, 40 mm i. d.), a quartz reactor (600 mm length, 60 mm i. d.), a quartz tube (15 mm i. d.), an ice− water bath for condensation and a sample bag for gas collection. For each pyrolysis trial, 2 g algae and 20 g alkali carbonates were mixed uniformly to ensure sufficient contact in advance and loaded into the corundum crucible, and then hung together in the heating zone of the electric furnace with a stainless-steel wire. N_2 (400 mL/min, purity >99.9%) was introduced into the quartz reactor for 15 min to create an oxygen-free condition, and adjusted to 100 mL/min before the reaction began. Next, the mixture of algae and salts was heated to the targeted temperatures (800, 850 and 900 °C) at a heating rate of 15 °C/min and kept at the target temperatures for 1 h. Finally, the corundum crucible was cooled under N_2 atmosphere to obtain the py-rolysis product. The slow heating rate was adopted, which is different from the existing researches (Lu et al., 2016a,b,c; Yin et al., 2014), mainly because carbon yield is higher at a lower heating rate.

After the reaction, the corundum crucible containing the mixture was first immersed in a beaker containing 0.5 M HCl (about 150 mL) for 4 h to remove the remaining carbonates and part of ash in raw algae. The mixed solution composed of HCl, chlorate and solid particles was then vacuum filtered using deionized water for six times, the as-received carbon was further vacuum-dried at 85 °C for 12 h and weighted to obtain the carbon yield. The final ACs were denoted as X-T, where X represented the reaction medium (A: Na_2CO_3–K_2CO_3–Li_2CO_3, B: Na_2CO_3–K_2CO_3) and T represented the target temperature (800, 850 and 900 °C). Additionally, for comparison, pyrolysis experiments with quartz sand (C-900) and without reaction medium (D-900) were also carried out.

2.3. Characterization of ACs

The characteristics of pyrolysis process with different reaction mediums was analyzed with a thermal gravimetric analyzer (Pyris1 TGA, Shanghai, China). To simulate the actual pyrolysis processes, the weight loss was recorded in the range of 30–915 °C at a heating rate of 15 °C/ min under a nitrogen flow rate of 100 mL/min.

The morphology of the ACs was measured by field emission scanning electron microscopy (FE-SEM, Nova NanoSEM 450, Holland), the ulti-mate analysis was measured using an elemental analyzer (Vario EL Cube, Germany), and the surface element composition and configura-tions of the samples were performed on X-Ray Photoelectron Spectros-copy (XPS, EscalLab 250Xi, America). Fourier transform infrared spectroscopy (FTIR) analyzer (Invenio-R, Germany) was used to detect the surface functional groups, Raman spectroscopy (LabRAM HR800, France) was employed to analyze the carbon structure, and X-ray diffraction spectroscopy (XRD, SmartLab-SE, Japan) was further used to characterize the crystal structure of the carbon with Cu Kα radiation at $\lambda = 1.5406$ Å.

The pore characteristics of ACs was detected by introducing a Micromeritics ASAP 2020 analyzer through the N_2 isothermal adsorption measured at 77 K. The specific surface area (SSA) was calculated using the adsorption curve from 0.05 to 0.25 P/P_0 by the Brunauer-Emmett-Teller (BET) method; the total pore volume was calculated from the adsorption value at 0.99; the micropore volume was obtained using the t-plot method; and the pore size distributions was established based on the density functional theory (DFT) method.

2.4. Electrochemical measurements

All the electrochemical measurements were performed in a 6 M KOH solution on a Shanghai Chenhua electrochemical workstation (CHI760E, China). For the three-electrode system, a platinum sheet and a KCl saturated calomel electrode was used as the counter electrode and the reference electrode respectively. The ACs (2 ± 0.1 mg), acetylene black and polytetrafluoroethylene (dissolved in N-methyl-2-pyrrolidone) were mixed with a mass ratio of 8:1:1 to make a slurry, which was then pressed on a nickel foam current collector for the working electrode preparation. The cyclic voltammetry (CV) and the galvanostatic charge/ discharge (GCD) tests were conducted in the potential range of − 0.8–0.2 V, and the electrochemical impedance spectroscopy (EIS) was measured in a frequency range from 10 mHz to 100 kHz at open circuit potential of 5 mV voltage amplitude.

The specific capacitance (C, F/g) of the ACs in the three-electrode system is calculated as follows:

$$C = \frac{I \times \Delta t}{m \times \Delta V} \quad (1)$$

where I is the applied constant current (A), Δt is the discharge time (s), m is the mass of ACs (g) and ΔV is the potential change excluding the IR ohmic drop.

3. Results and discussion

3.1. Pyrolysis process

To investigate the pyrolysis process and identify the effect of different reaction medium, the thermogravimetric (TG) and the differential thermogravimetric (DTG) experiments were conducted at the mass ratio of algae to media mass ratio of 1:10, and the results are presented at Fig. 1 and S2. In general, conventional algae pyrolysis process (Fig. 1a) can be divided into three stages, namely drying stage (40–140°C), pyrolysis stage (140–500°C) and carbonization stage (500–900°C) (Kong et al., 2022). The drying stage is primarily due to the evaporation of external water and small molecule compounds, the py-rolysis stage with the maximum mass loss is associated with the rapid decomposition of proteins, carbohydrates and lipids, and the pyrolysis stage is attributed to the degradation of fixed carbon (Kong et al., 2022).

As is seen from Fig. 1a and b, the addition of molten salts causes a large weight loss at the drying stage mainly due to the moisture absorption of carbonates. And in the pyrolysis stage, carbonates decrease the temperature corresponding to the maximum weight loss rate by about 20 °C (TS) and 25 °C (BS) respectively, which is attributed to the catalytic performance of carbonates (Li et al., 2020; Zeng et al., 2020; Zhang et al., 2022). Researches have shown that Na_2CO_3 and K_2CO_3 had

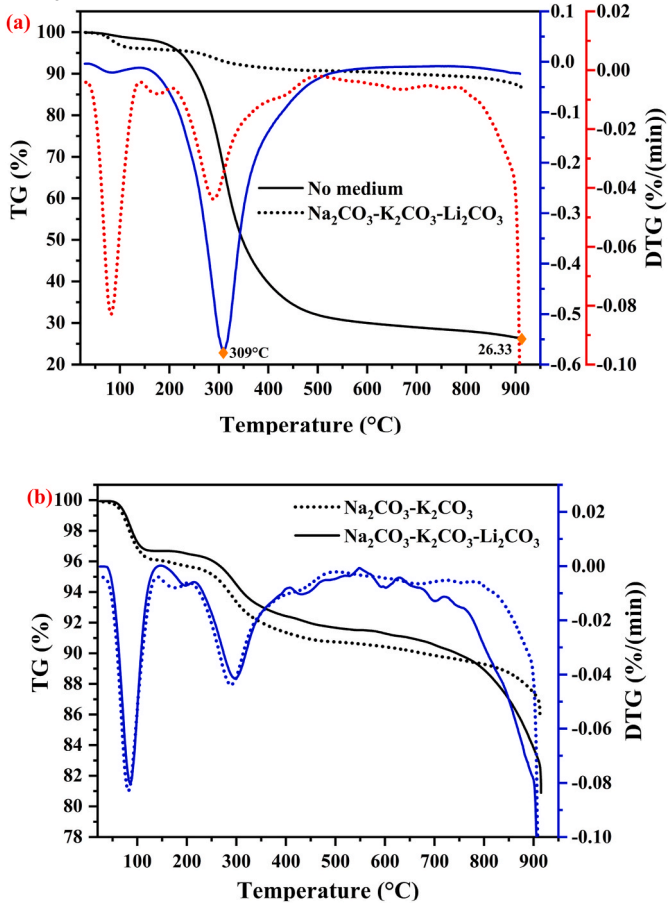

Fig. 1. Differences in TG and DTG curves of (a) Na_2CO_3–K_2CO_3 and no medium systems, (b) Na_2CO_3–K_2CO_3 and Na_2CO_3–K_2CO_3–Li_2CO_3 systems.

a distinct catalytic effect in prompting the biomass decomposition between 150 °C and 350 °C, such as the hydrolysis and depolymerization of cellulose and hemicellulose, and the dehydration and polymerization of monosaccharides (Zhao et al., 2017; Díez et al., 2019), which is not available with Li_2CO_3. At temperature lower than 780 °C, the weight loss of BS is always larger than that of TS, which may be caused by different moisture absorption or better catalytic performance of molten Na_2CO_3–K_2CO_3. This trend reverses when the temperature exceeds 780 °C, TS shows a larger weight loss mainly due to the decomposition of Li_2CO_3 and the redox reaction between Li_2CO_3 and carbon (Nagase et al., 1999; Zeng et al., 2021). Both BS and TS have a sharp weight loss at around 880 °C, which has been confirmed to be decomposition and evaporation of carbonates rather than carbon/carbonate gasification (Jalalabadi et al., 2020). It should be pointed out that the challenge of carbonates decomposition at high temperature can be solved by feeding H_2O and CO_2 generated by decomposition to regenerate carbonates (Raharjo et al., 2013).

On the other hand, quartz sand also reduces the temperature corresponding to the maximum weight loss rate by about 3 °C while maintaining the same solid residual amount (close to 26 wt% after normalization) compared with conventional pyrolysis. This may be because the good thermal conductivity of quartz sand improves the temperature uniformity and facilitates the volatile releasing. It also suggests that it is not suitable for ACs production by enhancing heat transfer through traditional solid particles alone.

Carbon yields after pyrolysis of algae are listed in Table S1. Conventional and quartz sand pyrolysis at 900 °C obtains a high carbon yield of 25.66 wt% and 25.54 wt%, which agrees well with the results ob-tained by TG (Fig. 1a). Compared with conventional pyrolysis, BS and TS reduce carbon yield by 10.6 wt% and 14.6 wt% respectively mainly due to the reaction (shown in Eq. (2)) between carbon and carbonates (Nagase et al., 1999), as well as a good solubility of molten carbonates for ashes such as silicates and metal ions(Mitsuoka et al., 2011). As temperature rises from 800 °C to 900 °C, the carbon yield of BS grad-ually decreases to 15.05 wt%, this trend is similar to the existing findings (Yin et al., 2014). Besides, BS shows a higher carbon yield than that of TS. It is likely that Na_2CO_3–K_2CO_3–Li_2CO_3 completely melts at tem-perature higher than 850 °C, forming a large number of alkali metal ions that can enter the interior of carbon to promote its decomposition, while Na_2CO_3–K_2CO_3 melts incompletely.

$$CO_3^{2-} + C \rightarrow O^{2-} + 2CO \quad (2)$$

3.2. Physicochemical characterization

The morphology of ACs is observed by FE-SEM. As shown in Fig. 2, D- 900 is lumpy pieces with rough surface and few pores. C-900 is in the form of flakes with a large number of regular quadrilateral shallow holes on surface, this similar phenomenon was also observed by Dai et al. in the process of quartz sand pyrolysis(Binyu et al., 2017). It can be explained that carbon is formed attaching to the surface of agglomerated quartz sand, which is easy to detach from carbon surface to form shallow holes due to its reduced expansibility when the temperature drops from high temperature. Due to the activation effect of carbonates, A-900 mainly exhibits small lumps with abundant pores on the surface(Lu et al., 2016a,b,c).

As displayed in Fig. 3, B-800 mainly consists of small blocks and strips, which gradually transform into a fluffy flocculent structure with more abundant pores and larger surface area as temperature increases. It can be concluded that temperature above 800 °C is necessary for Na_2CO_3–K_2CO_3 activation. On the other hand, B-900 presents better porosity and larger surface area compared to A-900. Na_2CO_3–K_2CO_3 exhibits better activation effect than Na_2CO_3–K_2CO_3–Li_2CO_3 because more K_2CO_3 and Na_2CO_3 are involved in the pyrolysis process under the same salt loading(Yin et al., 2014). In summary, Na_2CO_3–K_2CO_3 exhibits better performance for harvesting capacitive carbon from algae

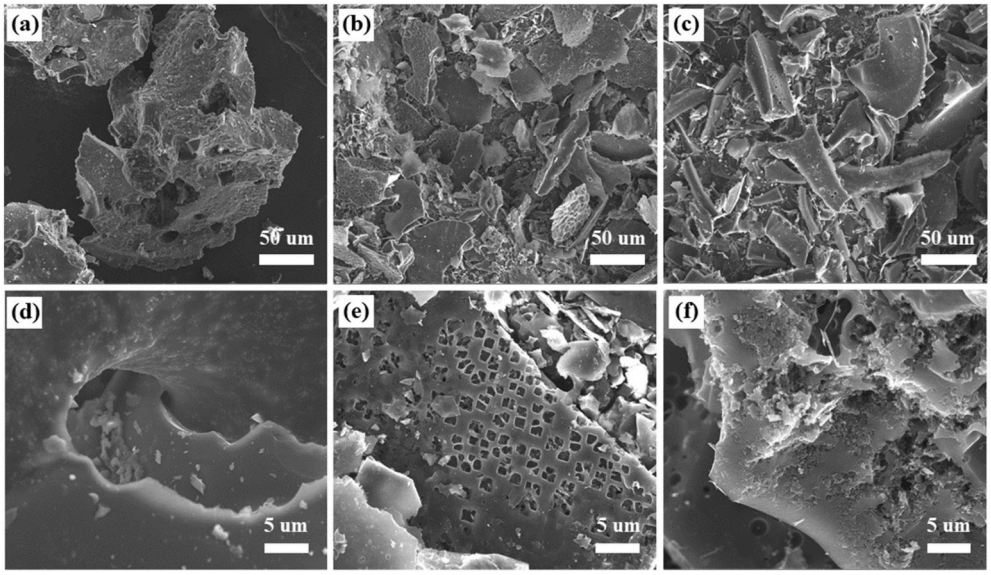

Fig. 2. FE-SEM images of (a, d) D-900; (b, e) C-900; (c, f) A-900.

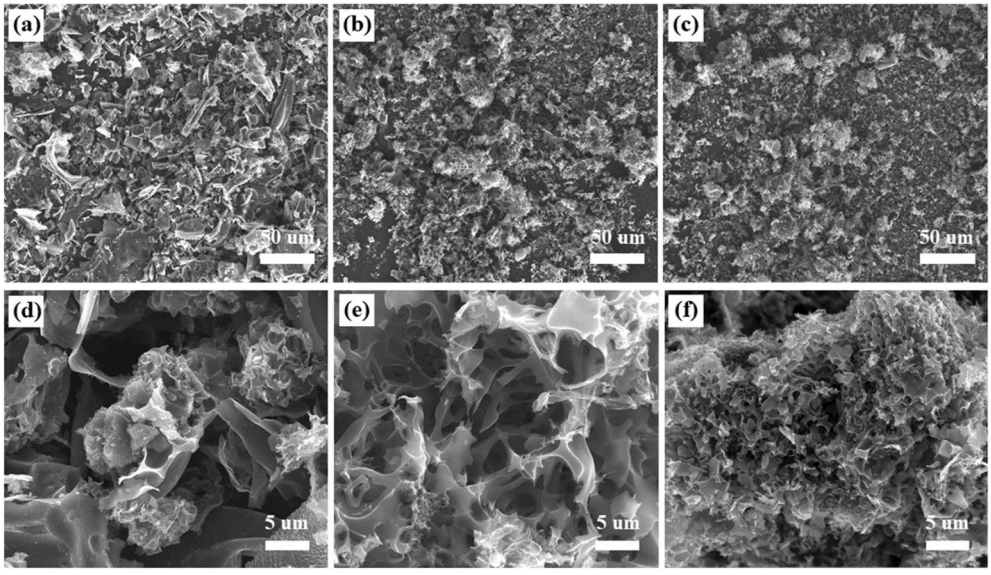

Fig. 3. FE-SEM images of (a, d) B-800; (b, e) B-850; (c, f) B-900.

pyrolysis both in terms of higher carbon yield and superior morphology.

To further reveal the morphological properties, the N_2 adsorption-desorption isotherms of the ACs are shown in Fig. 4. On this basis, the pore size distribution presented in Fig. S3 is evaluated by the density functional theory (DFT) method. D-900 and C-900 exhibit poor pore structure, while other four carbons prepared with molten salts exhibit type I/IV isotherm with typical H4 hysteresis loops ($0.4 < P/P_0 < 0.99$), corresponding to the existence of substantial mesopores(Lu et al., 2017). In addition, these four curves all show a rapid upward trend in the P/P_0 regions of 0–0.2 and 0.9–1.0, which are characteristics of microporous and macroporous structures, respectively(Zou et al., 2020). The results indicate that the ACs possess a hierarchical porous structure, which is consistent with the FE-SEM images and the pore size distribution (Fig. S3), in which the most prominent pores are distributed in the re-gion of 1–5 nm. It was reported that this hierarchical porous structure can contribute to the electrolyte ion diffusion and ion storage, thereby improving the utilization efficiency of specific surface area (SSA) and increasing its specific capacitance(Hou et al., 2015; Wu et al., 2020).

The detailed pore parameters of the ACs are presented in Table 1. The SSA of D-900 is 3.30 m^2/g with pore volume (V_{total}) of 0.019 cm^3/g and no micropores, indicating that the carbon obtained by algae py-rolysis without reaction medium needs to be activated. Quartz sand increases SSA, V_{total} and $V_{micropore}$ slightly, but still far from being suitable for capacitive carbon production. The introduction of molten carbonates significantly increases SSA to 1450–2050 m^2/g, V_{total} to 0.75–1.1 cm^3/g, and $V_{micropore}$ to 0.48–0.74 cm^3/g. This is because molten carbonates can enhance the fragmentation of algae pyrolysis intermediates in pyrolysis process, promoting the reorganization of the solid matrix, as well as the development of microstructure (Kalderis et al., 2008; Liu et al., 2022; Nzihou et al., 2013). In the case of BS, the SSA, V_{total} and $V_{micropore}$ are positively correlated with temperature, and their maximum values can reach 2009.26 m^2/g, 1.064 cm^3/g and 0.735 cm^3/g respectively at 900 °C. Therefore, high temperatures around 900 °C is recommended to harvest carbon with superior structure for algae pyrolysis with Na_2CO_3–K_2CO_3.

The XRD spectrum displayed in Fig. 5a reveals the crystalline

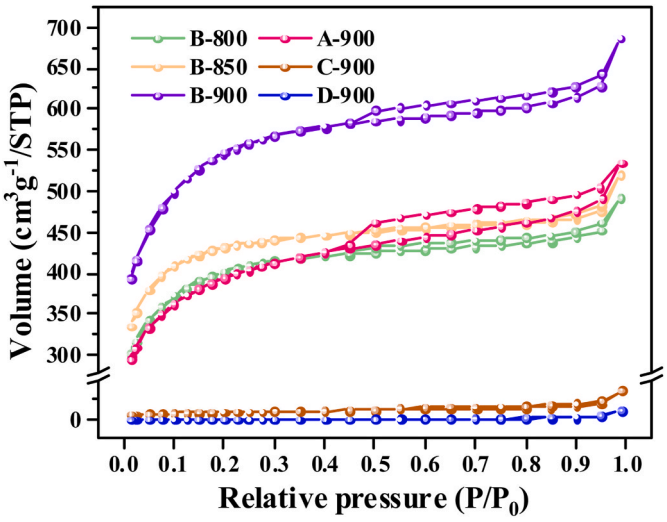

Fig. 4. Nitrogen adsorption–desorption isotherms of the ACs.

Table 1
Pore characteristics and carbon yields under different conditions.

Samples	SSA (m^2/g)	V_{total} (cm^3/g)	$V_{micropore}$ (cm^3/g)
B-800	1491.95	0.761	0.540
B-850	1637.01	0.806	0.613
B-900	2009.26	1.064	0.735
A-900	1454.08	0.828	0.484
C-900	35.67	0.057	0.008
D-900	3.30	0.019	0.000

SSA, specific surface area; V, volume.

changes of carbon. The broadened diffraction peaks (21–25°) and the small diffraction peaks (43°) correspond to the (002) plane of graphite lattice and the (100) plane of graphite respectively, suggesting that the ACs are all typical amorphous carbon structures (Wang et al., 2020a,b). It can be found that the (002) peak of the carbon obtained by molten salt is more diffused, especially at higher temperatures. This result can be explained as the rearrangement of carbon atom to graphitic crystalline is retarded by molten carbonates, forming less ordered carbon which is conducive to generate more pores and defects(Liang et al., 2021; Nayak et al., 2017).

The Raman spectra of the carbon structure is presented in Fig. 5b, the D peak (1350 cm^{-1}) belongs to the disordered or defective graphite structure and the G peak (1580 cm^{-1}) is attributed to the sp^2 hybrid carbon atom(Zou et al., 2020). The I_D/I_G value (the intensity ratio of D peak and G peak, all calculated on average of three test results) generally represents the extent of graphitic disorder in carbon materials. Although, all the carbons share I_D/I_G value around 1.0, molten car-bonates and higher temperatures lead to a higher number of defects in carbon, which is conducive to the surface charge storage(Zhou et al., 2020).

FTIR analysis (Fig. 6) is carried out to investigate the functional groups of the raw algae and the ACs, and assignment of the absorption bands is done based on the existing literatures with results shown in Table S2(Aboulkas et al., 2017; Lin et al., 2017). The primary bands of raw algae appear at 3294, 2937, 1662, 1540, 1396, 1242 1054 and 705 cm^{-1} respectively, due to the abundant content of proteins, lipids and carbohydrates. The bands of carbons mainly distribute at 3428, 1637, 1396, 1180, 1054 and 802 cm^{-1}.

The peaks at 3428 cm^{-1} are particularly obvious for all carbons, which shift to a higher wavelength compared with that of raw algae (3294 cm^{-1}), which may be caused by the sharp decrease of amine groups after pyrolysis, while the O–H bands keep relatively stable. As for

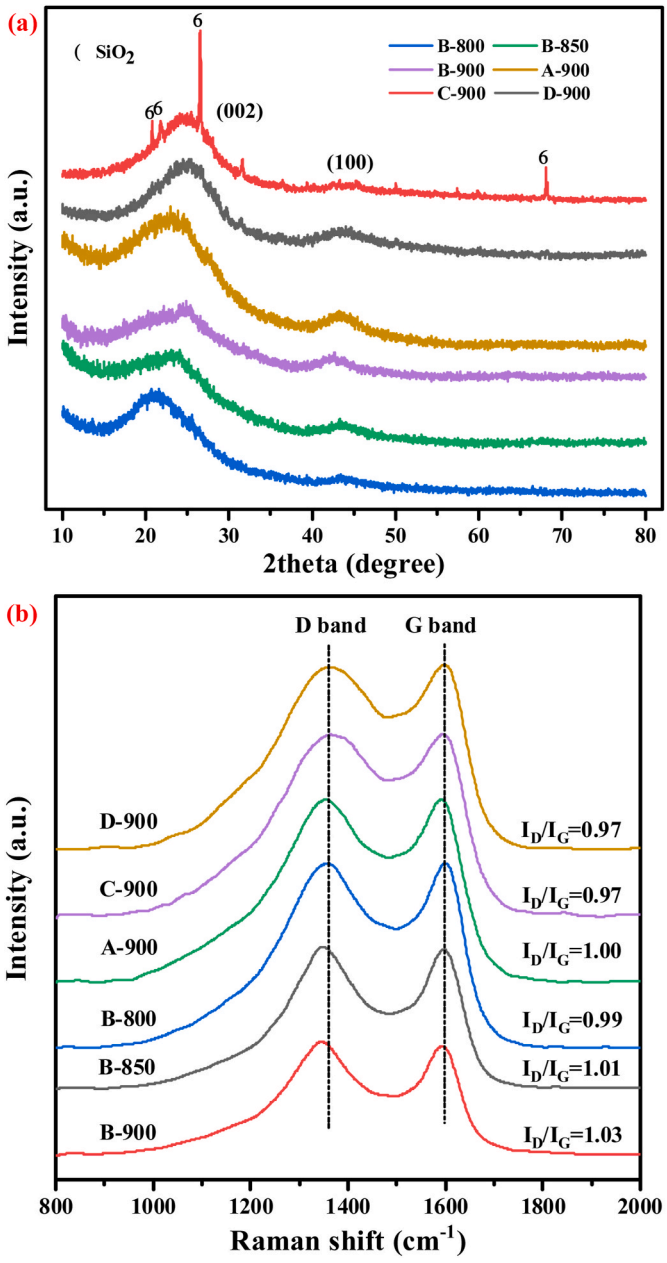

Fig. 5. (a) XRD patterns; (b) Raman spectra of the ACs.

carbon, the peaks appear at 1637 and 802 cm^{-1} is mainly due to the increase of carbon aromaticity caused by the polymerization and cyclization reaction(Chen et al., 2017b), while peaks at 1662 and 1540 cm^{-1} almost disappear due to the cleavage of C–N bonds resulting from the decomposition of amino acids at high temperature(Chen et al., 2017a; Xie et al., 2020). The addition of molten carbonates significantly reduces the C–H peaks at 2937 and 1242 cm^{-1}, as molten carbonates could promote the demethylation and the cracking of carbon framework(Chen et al., 2021). The peak at 1092 cm^{-1} replaces the peak at 1180 and 1054 cm^{-1}, indicating that the oxygen in carbon is more stable in the form of phenol bonds after pyrolysis with molten salt. It should be noted that C-900 and D-900 or A-900 and B-900 exhibit nearly identical spectra, suggesting that the enhancement of temperature uniformity or the molten carbonates composition would not change the functional group types at high temperature around 900 °C. The element content, as well as the surface elemental properties of the carbon obtained at 900 °C are further characterized by combined elemental analysis and XPS analysis. As displayed in Table S3, the

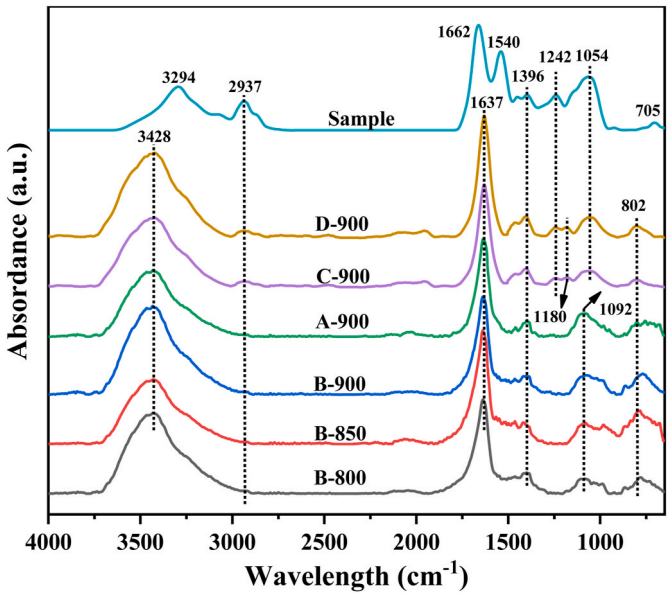

Fig. 6. FTIR spectra of the raw algae and ACs.

nitrogen content (about 1.2 wt%) is greatly reduced after pyrolysis especially for B-900 and A-900, which corresponds to the disappearance of the Amide I and Amide II bonds mentioned above (Peng et al., 2023). Although molten salt promotes the nitrogen releasing during the py-rolysis process, the nitrogen content of the ACs is still much higher than that of most raw biomass(Vassilev et al., 2010), which is beneficial to improve the capacitance of carbon.

As can be seen from Fig. 7 and Fig. S4–S6, there are three typical peaks in XPS spectra for all samples, mainly located at about 285, 400, and 533 eV, ascribed to C 1s, N 1s and O 1s peak, respectively. In general, the high-resolution C 1s spectra can be primarily referred to C–C/C C/C–H (285.0 eV), C–O/C–O–C/C N (286.0 eV), C O/N–C–O (287.8 eV) and CO_3^{2-} (289.5 eV, molten salt residue)(Chen et al., 2017b; Hammond et al., 1981). Molten salts promote the complete cleavage of C O/N–C–O bond, where the change of C O bond corresponds to the removal of the Amide I bond in FTIR results. The N 1s spectra can be recognized as pyridinic–N (398.5 eV), protein–N (400.0 eV), pyrrolic–N (400.6 eV), quaternary–N (401.3 eV) and oxidized–N (403.0 eV)(Ma et al., 2022; Tian et al., 2013). The small amount of oxidized–N present in conventional pyrolysis carbon is completely removed in molten salt. Moreover, BS-900 contains pyrrolic–N and quaternary–N, which enhance the surface charge storage and improve the electronic con-ductivity respectively, both playing a positive role in the preparation of capacitive carbon materials(Sun et al., 2018; Zhou et al., 2017). The O 1s spectra is deconvoluted into C O (531.9 eV), O–C O/–OH (532.4 eV), O–C O/C=O (533.5 eV) and adsorbed O (536.5 eV)(Wang et al., 2020a, b). Also, the carbonyl type and hydroxyl type oxygen-containing groups in BS-900 can help to improve the pseudo-capacitive performance to some degree(Wu et al., 2020).

3.3. *Electrochemical performance*

Based on the structure and functional group properties discussed above, the capacitive performance of the ACs, especially B-900, is evaluated for supercapacitor electrode materials. Fig. 8a presents the CV curves of all samples recorded at 100 mV/s in the voltage window of − 0.8 to 0.2 V. It can be clearly found that the carbon obtained with molten salts take roughly rectangular shapes and the CV profile of B-900

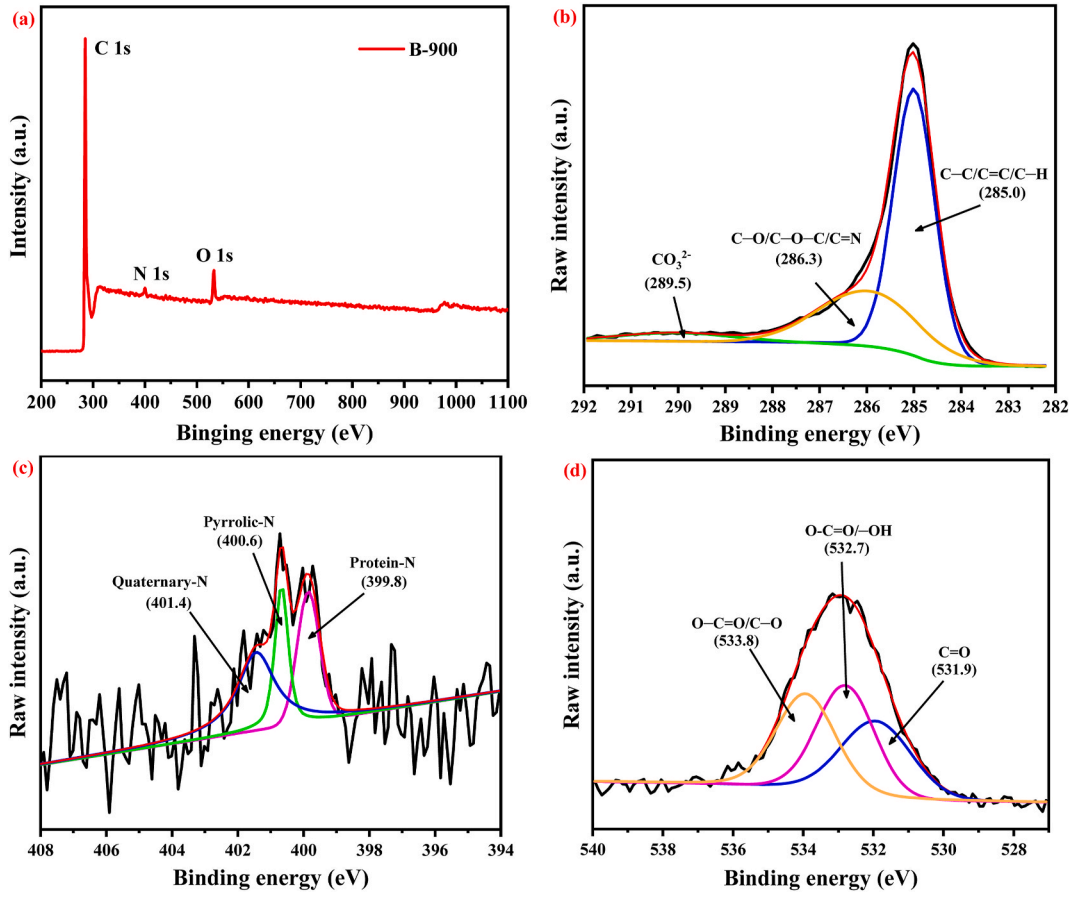

Fig. 7. (a) XPS survey spectra, (b) high-resolution XPS C1s spectra, (c) high-resolution XPS N1s spectra and (d) high-resolution XPS O1s spectra of B-900.

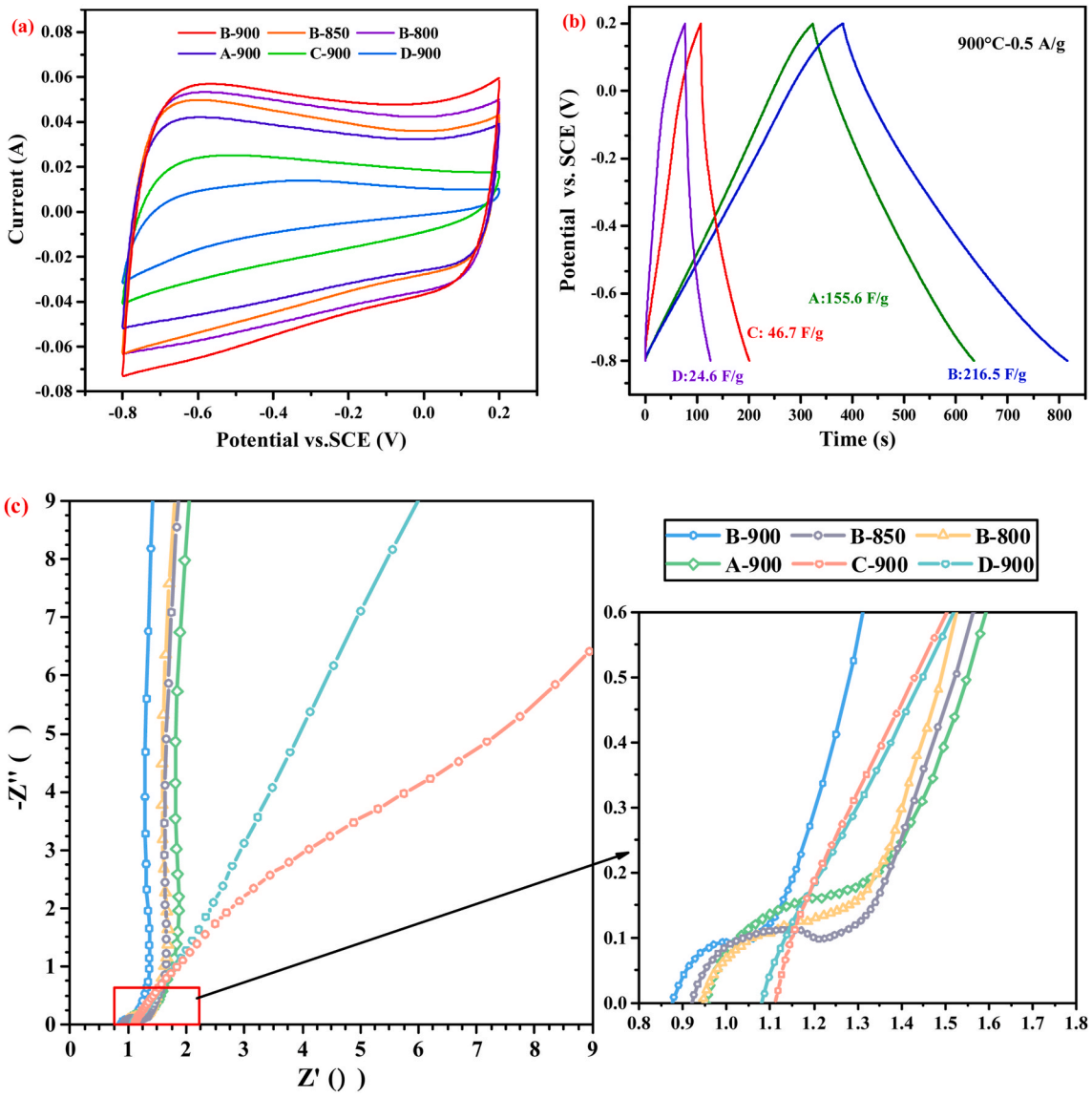

Fig. 8. (a) CV curves at 100 mV/s; (b) GCD curves; (c) Nyquist plots.

obviously possesses the best rate performance. The weakly broadened humps appearing at the potential range of − 0.8 to − 0.2V may be associated with pseudo-capacitance caused by some functional groups on the surface of carbon(Zou et al., 2020), such as the oxygen- and nitrogen-containing functional groups demonstrated by XPS above. In addition, the current changes sharply at the switching potential, which means less resistance to mass transfer at the electrodes(Wang et al., 2017), mainly benefiting from the hierarchical porous structure.

As shown in Fig. 8b, the carbons obtained from different reaction medium at 900 °C have different GCD curves (current density: 0.5 A/g), indicating a significant difference in the capacitance. The imperfect symmetry of these curves further confirms the small amount of pseudo- capacitance introduced by heteroatom functional groups(Wang et al., 2017). In addition, B-900 shows the highest specific capacitances of 230.2 F/g at 0.25 A/g, which directly confirms the superiority of Na_2CO_3–K_2CO_3 to harvest the capacitive carbon.

Fig. 8c presents the Nyquist plots of the EIS for all carbons. In the low frequency region, the electrodes prepared by the carbon obtained with molten salts all exhibit nearly straight lines, demonstrating a low equivalent resistance of ion diffusion and mobility(Gao et al., 2021). In the high frequency region, the diameter of the semicircle stands for the charge transfer resistance (R_{ct}), B-900 shows a R_{ct} value of ~0.11 Ω, which is much lower than that of B-800 (~0.20 Ω), B-850 (~0.18 Ω) and A-900 (~0.27 Ω). In addition, the axis intercept represents the electro-de/electrolyte contact resistance (R_s), and B-900 possesses the lowest R_s value of about 0.88 Ω. Overall, the low R_{ct} and R_s values explain the best rate performance of B-900.

Fig. 9a and b further demonstrates the CV curves and GCD curves of B-900 at the scan rate of 10–100 mV/s and current density of 0.25–2 A/g, respectively. The rectangular-shaped character of the CV curve is well maintained at these scan rates, suggesting the ideal capacitive behavior of B-900. The specific capacitance is as high as 173.9, 194.8, 216.5 and 230.2 F/g under a current density of 2, 1, 0.5 and 0.25 A/g, respectively. And as the current density increased from 0.25 to 2 A/g, the capacitance retention remains at 75.54%. Moreover, the B-900-based electrode ex-hibits good cyclic stability with 90.4% retention after 5000 cycles at 1 A/g (Fig. 9c). In order to evaluate the capacitance performance of the B-900 electrode, the plots of capacitance versus current density, along with the results from other studies are presented in Fig. 9d. B-900 has a specific capacitance range of 173.9–230.2 F/g, which is superior to the previously reported data for other carbon electrode prepared by biomass pyrolysis with Na_2CO_3–K_2CO_3(Liu et al., 2021; Lu et al., 2016a,b,c; Yin et al., 2014).

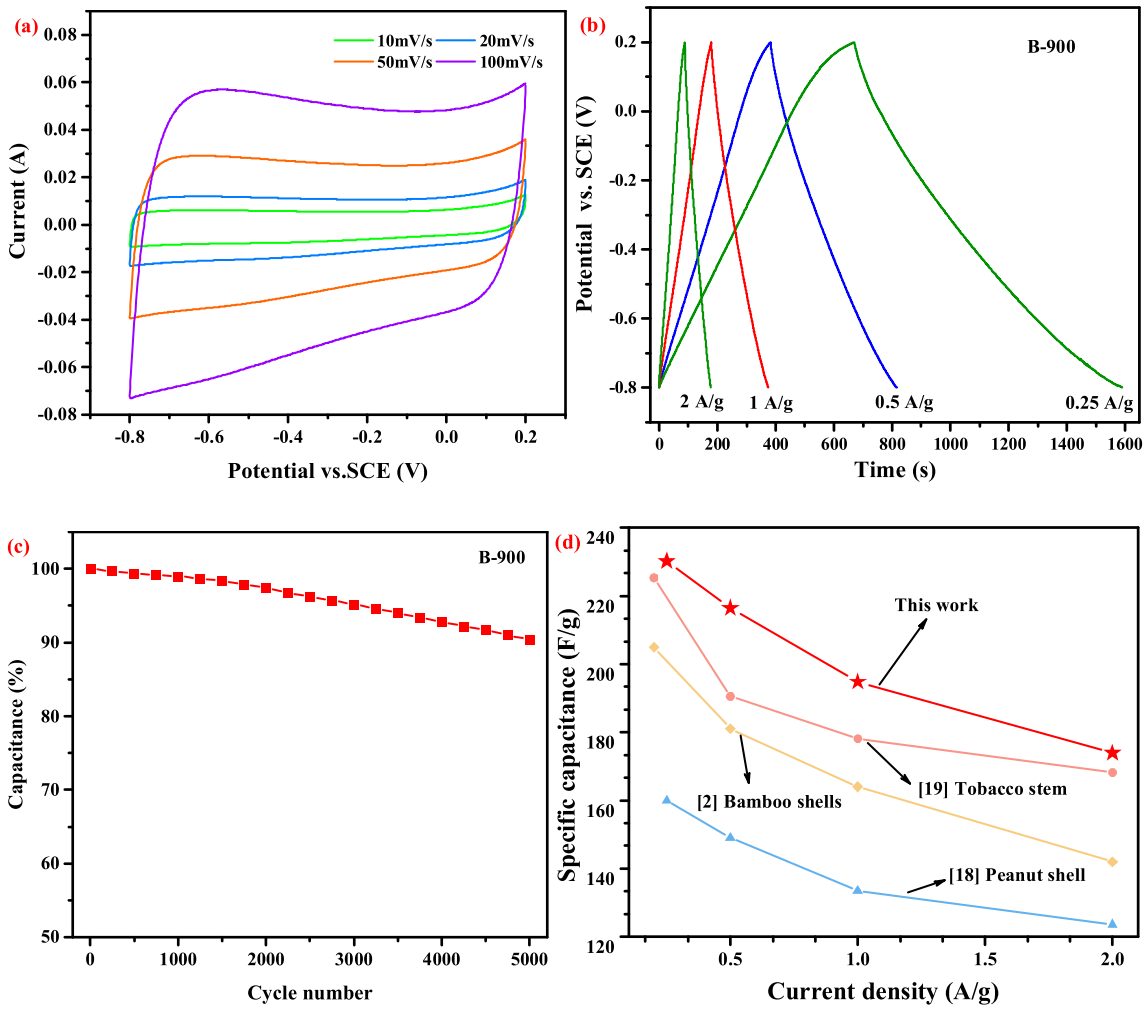

Fig. 9. (a) CV curves; (b) Charge-discharge curves; (c) Cycling stability in a three-electrode system; Charge-discharge curves; (d) Plot of capacitance as a function of current density and results for other biomass.

3.4. Outlooks

The carbon materials obtained by algae pyrolysis in molten carbonates show excellent capacitive performance and is an ideal material for the preparation of supercapacitor electrodes. However, the nitrogen content of the as-prepared carbon is 1.2 wt%, which is higher than the nitrogen content of most biomass but much lower than that of algae used in this study. It is well known that nitrogen doping can improve the capacitance of carbon in terms of charge density and polarity. Therefore, the evolution of nitrogen during algae pyrolysis in molten carbonates is urgent to study in order to provide guidance for fixing more nitrogen in carbon by appropriate means, such as the heating rate control of multi- stage (Yang et al., 2023). The as-prepared carbon in this paper possesses superior porosity and specific surface area, and it also has the potential to be applied for oxygen reduction reaction (ORR, provides accessible active sites and facilitates mass transport in catalyst layers) and adsor-bent, which is also worth exploring in the future. In addition, the energy flow analysis of the system will also help to elucidate the clean char-acteristics of the solar pyrolysis (e.g. CO_2 reduction capacity), such as reducing the reflection coefficient of solar reactor materials (see Scheme 1 in the supplementary material).

4. Conclusion

Molten salt promotes the volatiles releasing during pyrolysis, but also reduces the yield and graphitic disorder of carbon, as well as the nitrogen content in carbon, to a certain extent. Na_2CO_3–K_2CO_3 is proven to be an effective chemical activator for algae pyrolysis process. Temperature above 800 °C is essential for its catalytic performance, and high temperature around 900 °C is favorable for harvesting capacitive carbon both in terms of carbon yield and superior morphology. The obtained B-900 shows a high specific surface area (2009.26 m^2/g) with abundant hierarchical pores (mainly micropores and mesopores) and oxygen and nitrogen doping carbon structure (pyrrolic–N, quaternary–N, C═O and –OH). B-900 possesses a high specific capacitance of 230.2 F/g at 0.25 A/g, and its capacitance retention at 2 A/g can still remain 75.54%. Solar pyrolysis of algae in molten Na_2CO_3–K_2CO_3 is a green and promising process to harvest ACs with high specific capacitance.

CRediT authorship contribution statement

Jun Li: Writing – original draft, Software, Visualization. **Jing Peng:** Software, Visualization. **Kuo Zeng:** Writing – review & editing, Formal analysis. **Dian Zhong:** Methodology, Software. **Kang Xu:** Methodology, Investigation. **Vasilevich Sergey Vladimirovich:** Conceptualization, Formal analysis. **Ange Nzihou:** Methodology, Formal analysis. **Haiping Yang:** Methodology, Validation. **Hanping Chen:** Validation.

Declaration of competing interest

The authors declare that they have no known competing financial interests or personal relationships that could have appeared to influence

the work reported in this paper.

Data availability

Data will be made available on request.

Acknowledgement

Authors acknowledge funding from the National Natural Science Foundation of China (52111530296, 52261135626), and the support of National Natural Science Funds for Distinguished Young Scholar (52125601). In addition, authors would like to thank the Analytical and Testing Center in Huazhong University of Science & Technology (htt p://atc.hust.edu.cn) and the shiyanjia lab (https://www.shiyanjia. com) for the test. There are no conflicts to declare.

Appendix A. Supplementary data

References

Aboulkas, A., Hammani, H., El Achaby, M., Bilal, E., Barakat, A., El Harfi, K., 2017. Valorization of algal waste via pyrolysis in a fixed-bed reactor: production and characterization of bio-oil and bio-char. Bioresour. Technol. 243, 400–408. https://10.1016/j.biortech.2017.06.098.

Binyu, D., Hongwei, H., Haiqing, L., 2017. Mechanism of inproving strength of resin sand by high temperature baking. Special Castion & Nonferrous alloys 37, 12–14.

Chen, H., Tang, Z., Liu, B., Chen, W., Hu, J., Chen, Y., Yang, H., 2021. The new insight about mechanism of the influence of K_2CO_3 on cellulose pyrolysis. Fuel 295, 120617. https://10.1016/j.fuel.2021.120617.

Chen, W., Yang, H., Chen, Y., Xia, M., Chen, X., Chen, H., 2017a. Transformation of nitrogen and evolution of N-containing species during algae pyrolysis. Environ. Sci. Technol. 51, 6570–6579. https://10.1021/acs.est.7b00434.

Chen, W., Yang, H., Chen, Y., Xia, M., Yang, Z., Wang, X., Chen, H., 2017b. Algae pyrolytic poly-generation: influence of component difference and temperature on products characteristics. Energy 131, 1–12. https://10.1016/j.energy.2017.05.019.

Díez, N., Ferrero, G.A., Fuertes, A.B., Sevilla, M., 2019. Sustainable salt template-assisted chemical activation for the production of porous carbons with enhanced power handling ability in supercapacitors. Batteries & Supercaps 2, 701–711. https://doi.org/10.1002/batt.201900037.

Dong, L., Xu, C., Li, Y., Huang, Z., Kang, F., Yang, Q., Zhao, X., 2016. Flexible electrodes and supercapacitors for wearable energy storage: a review by category. Journal of materials chemistry. A, Materials for energy and sustainability 4, 4659–4685. https://10.1039/c5ta10582j.

Gao, Y., Sun, R., Li, A., Ji, G., 2021. In-situ self-activation strategy toward highly porous biochar for supercapacitors: direct carbonization of marine algae. J. Electroanal. Chem. 882, 114986. https://10.1016/j.jelechem.2021.114986.

Giwa, A., Yusuf, A., Ajumobi, O., Dzidzienyo, P., 2019. Pyrolysis of date palm waste to biochar using concentrated solar thermal energy: economic and sustainability implications. Waste Manage. (Tucson, Ariz.) 93, 14–22. https://doi.org/10.1016/j.wasman.2019.05.022.

Hammond, J.S., Holubka, J.W., DeVries, J.E., Dickie, R.A., 1981. The application of x-ray photo-electron spectroscopy to a study of interfacial composition in corrosion-induced paint de-adhesion. Corrosion Sci. 21, 239–253. https://doi.org/10.1016/0010-938X(81)90033-0.

Hou, J., Cao, C., Idrees, F., Ma, X., 2015. Hierarchical porous nitrogen-doped carbon nanosheets derived from silk for ultrahigh-capacity battery anodes and supercapacitors. ACS Nano 9, 2556–2564. https://10.1021/nn506394r.

Jalalabadi, T., Moghtaderi, B., Allen, J., 2020. Thermochemical conversion of biomass in the presence of molten alkali-metal carbonates under reducing environments of N_2 and CO_2. Energies 13, 5395. https://10.3390/en13205395.

Kalderis, D., Bethanis, S., Paraskeva, P., Diamadopoulos, E., 2008. Production of activated carbon from bagasse and rice husk by a single-stage chemical activation method at low retention times. Bioresour. Technol. 99, 6809–6816. https://10.1016/j.biortech.2008.01.041.

Kong, W., Shen, B., Ma, J., Kong, J., Feng, S., Wang, Z., Xiong, L., 2022. Pyrolysis of Spirulina platensis, Tetradesmus obliquus and Chlorella vulgaris by TG-FTIR and Py- GC/MS: kinetic analysis and pyrolysis behaviour. Energy 244, 123165. https://10.10 16/j.energy.2022.123165.

Law, X.N., Cheah, W.Y., Chew, K.W., Ibrahim, M.F., Park, Y., Ho, S., Show, P.L., 2022. Microalgal-based biochar in wastewater remediation: its synthesis, characterization and applications. Environ. Res. 204, 111966 https://doi.org/10.1016/j.jcis.2017.01.031.

Li, J., Xie, Y., Zeng, K., Flamant, G., Yang, H., Yang, X., Zhong, D., Du, Z., Chen, H., 2020. Biomass gasification in molten salt for syngas production. Energy 210, 118563. https://doi.org/10.1016/j.energy.2020.118563.

Liang, X., Liu, R., Wu, X., 2021. Biomass waste derived functionalized hierarchical porous carbon with high gravimetric and volumetric capacitances for supercapacitors. Microporous Mesoporous Mater. 310, 110659. https://10.1016/j.micromeso.2020.110659.

Lin, H., Wang, S., Zhang, L., Ru, B., Zhou, J., Luo, Z., 2017. Structural evolution of chars from biomass components pyrolysis in a xenon lamp radiation reactor. Chin. J. Chem. Eng. 25, 232–237. https://10.1016/j.cjche.2016.08.002.

Liu, D., Xu, G., Yuan, X., Ding, Y., Fan, B., 2023. Pore size distribution modulation of waste cotton-derived carbon materials via citrate activator to boost supercapacitive performance. Fuel 332, 126044. https://doi.org/10.1016/j.fuel.2022.126044.

Liu, Y., Cheng, X., Zhang, S., 2021. One-step molten salt carbonization of tobacco stem for capacitive carbon. J. Porous Mater. 28, 1629–1642. https://10.1007/s10934-021-01108-x.

Liu, Y., Tan, H., Tan, Z., Cheng, X., 2022. Rice husk derived capacitive carbon prepared by one-step molten salt carbonization for supercapacitors. J. Energy Storage 55, 105437. https://doi.org/10.1016/j.est.2022.105437.

Lobato-Peralta, D.R., Pacheco-Catalán, D.E., Altuzar-Coello, P.E., Béguin, F., Ayala-Cortés, A., Villafán-Vidales, H.I., Arancibia-Bulnes, C.A., Cuentas-Gallegos, A.K., 2020. Sustainable production of self-activated bio-derived carbons through solar pyrolysis for their use in supercapacitors. J. Anal. Appl. Pyrol. 150, 104901 https://doi.org/10.1016/j.jaap.2020.104901.

Lobato-Peralta, D.R., Ayala-Cortés, A., Longoria, A., Pacheco-Catalán, D.E., Okoye, P.U., Villafán-Vidales, H.I., Arancibia-Bulnes, C.A., Cuentas-Gallegos, A.K., 2022. Activated carbons obtained by environmentally friendly activation using solar energy for their use in neutral electrolyte supercapacitors. J. Energy Storage 52, 104888. https://doi.org/10.1016/j.est.2022.104888.

Lu, B., Hu, L., Yin, H., Mao, X., Xiao, W., Wang, D., 2016a. Preparation and application of capacitive carbon from bamboo shells by one step molten carbonates carbonization. Int. J. Hydrogen Energy 41, 18713–18720. https://10.1016/j.ijhydene.2016.08.083.

Lu, B., Hu, L., Yin, H., Mao, X., Xiao, W., Wang, D., 2016b. One-step molten salt carbonization (MSC) of firwood biomass for capacitive carbon. RSC Adv. 6, 106485–106490. https://10.1039/C6RA22191B.

Lu, B., Zhou, J., Song, Y., Wang, H., Xiao, W., Wang, D., 2016c. Molten-salt treatment of waste biomass for preparation of carbon with enhanced capacitive properties and electrocatalytic activity towards oxygen reduction. Faraday Discuss 190, 147–159. https://10.1039/C5FD00215J.

Lu, Y., Zhang, S., Yin, J., Bai, C., Zhang, J., Li, Y., Yang, Y., Ge, Z., Zhang, M., Wei, L., Ma, M., Ma, Y., Chen, Y., 2017. Mesoporous activated carbon materials with ultrahigh mesopore volume and effective specific surface area for high performance supercapacitors. Carbon 124, 64–71. https://doi.org/10.1016/j.carbon.2017.08.044.

Ma, X., Zhang, B., Xu, Z., Tan, Y., Li, B., Zhang, Y., Ni, G., Zhou, W., Luque, R., Zhang, H., 2022. N-rich and O-poor doped carbon prepared via facile ammonium nitrate assisted hydrothermal carbonization for robust supercapacitors. J. Clean. Prod. 373, 133903 https://doi.org/10.1016/j.jclepro.2022.133903.

Mao, Y., Xie, H., Chen, X., Zhao, Y., Qu, J., Song, Q., Ning, Z., Xing, P., Yin, H., 2020. A combined leaching and electrochemical activation approach to converting coal to capacitive carbon in molten carbonates. J. Clean. Prod. 248, 119218 https://doi.org/10.1016/j.jclepro.2019.119218.

Mitsuoka, K., Hayashi, S., Amano, H., Kayahara, K., Sasaoaka, E., Uddin, M.A., 2011. Gasification of woody biomass char with CO_2: the catalytic effects of K and Ca species on char gasification reactivity. Fuel Process. Technol. 92, 26–31. In: https:// 10.1016/j.fuproc.2010.08.015.

Nagase, K., Shimodaira, T., Itoh, M., Zheng, Y., 1999. Kinetics and mechanisms of the reverse Boudouard reaction over metal carbonates in connection with the reactions of solid carbon with the metal carbonates. Phys. Chem. Chem. Phys. 1, 5659–5664. https://10.1039/A906687J.

Naji, S.Z., Tye, C.T., 2022. A review of the synthesis of activated carbon for biodiesel production: precursor, preparation, and modification. Energy Convers. Manag. X 13, 100152. https://10.1016/j.ecmx.2021.100152.

Nayak, A., Bhushan, B., Gupta, V., Sharma, P., 2017. Chemically activated carbon from lignocellulosic wastes for heavy metal wastewater remediation: effect of activation conditions. J. Colloid Interface Sci. 493, 228–240. https://doi.org/10.1016/j.jcis.2017.01.031.

Nzihou, A., Stanmore, B., Sharrock, P., 2013. A review of catalysts for the gasification of biomass char, with some reference to coal. Energy 58, 305–317. https://10.1016/j.energy.2013.05.057.

Peng, J., Li, J., Zhong, D., Zeng, K., Xu, K., Gao, J., Nzihou, A., Zhang, X., Yang, H., Chen, H., 2023. Transformation of nitrogen during solar pyrolysis of algae in molten salt. Fuel Process. Technol. 242, 107664 https://doi.org/10.1016/j.fuproc.2023.107664.

Premarathna, K.S.D., Rajapaksha, A.U., Sarkar, B., Kwon, E.E., Bhatnagar, A., Ok, Y.S., Vithanage, M., 2019. Biochar-based engineered composites for sorptive decontamination of water: a review. Chem. Eng. J. 372, 536–550. https://10.1016/j.cej.2019.04.097.

Raharjo, S., Ueki, Y., Yoshiie, R., Naruse, I., 2013. Regeneration of used alkali carbonates for gaseous sulfur removal in a gasification system. Energy Fuel. 27, 2762–2766. https://10.1021/ef400219q.

Sun, F., Liu, X., Wu, H.B., Wang, L., Gao, J., Li, H., Lu, Y., 2018. In situ high-level nitrogen doping into carbon nanospheres and boosting of capacitive charge storage in both anode and cathode for a high-energy 4.5 V full-carbon lithium-ion capacitor. Nano Lett. 18, 3368–3376. https://10.1021/acs.nanolett.8b00134.

Tang, Z., Chen, W., Chen, Y., Hu, J., Yang, H., Chen, H., 2021. Preparation of low-nitrogen and high-quality bio-oil from microalgae catalytic pyrolysis with zeolites and activated carbon. J. Anal. Appl. Pyrol. 159, 105182. https://10.1016/j.jaap.2021.105182.

Tian, Y., Zhang, J., Zuo, W., Chen, L., Cui, Y., Tan, T., 2013. Nitrogen conversion in relation to NH_3 and HCN during microwave pyrolysis of sewage sludge. Environ. Sci. Technol. 47, 3498–3505. https://10.1021/es304248j.

Vassilev, S.V., Baxter, D., Andersen, L.K., Vassileva, C.G., 2010. An overview of the chemical composition of biomass. Fuel 89, 913–933. https://10.1016/j.fuel.2009.10 .022.

Velazquez-Lucio, J., Rodríguez-Jasso, R.M., Colla, L.M., Sáenz-Galindo, A., Cervantes-Cisneros, D.E., Aguilar, C.N., Fernandes, B.D., Ruiz, H.A., 2018. Microalgal biomass pretreatment for bioethanol production: a review. Biofuel Research Journal 5, 780–791. https://10.18331/BRJ2018.5.1.5.

Wang, C., Wu, D., Wang, H., Gao, Z., Xu, F., Jiang, K., 2017. Nitrogen-doped two-dimensional porous carbon sheets derived from clover biomass for high performance supercapacitors. J. Power Sources 363, 375–383. https://10.1016/j.jpowsour.2017.07.097.

Wang, Q., Qin, B., Li, H., Zhang, X., Tian, X., Jin, L., Cao, Q., 2020a. Honeycomb-like carbon with tunable pore size from bio-oil for supercapacitor. Microporous Mesoporous Mater. 309, 110551. https://10.1016/j.micromeso.2020.110551.

Wang, T., Rony, A.H., Sun, K., Gong, W., He, X., Lu, W., Tang, M., Ye, R., Yu, J., Kang, L., Luo, H., Smith, S.J., Eddings, E.G., Fan, M., 2020b. Carbon nanofibers prepared from solar pyrolysis of pinewood as binder-free electrodes for flexible supercapacitors. Cell Reports Physical Science 1, 100079. https://doi.org/10.1016/j.xcrp.2020.100079.

Wei, Y., Shen, C., Xie, J., Bu, Q., 2020. Study on reaction mechanism of superior bamboo biochar catalyst production by molten alkali carbonates pyrolysis and its application for cellulose hydrolysis. Sci. Total Environ. 712, 136435. https://10.1016/j.scitotenv.2019.136435.

Wu, J., Xia, M., Zhang, X., Chen, Y., Sun, F., Wang, X., Yang, H., Chen, H., 2020. Hierarchical porous carbon derived from wood tar using crab as the template: performance on supercapacitor. J. Power Sources 455, 227982. https://10.1016/j.jpowsour.2020.227982.

Xie, Y., Hu, W., Wang, X., Tong, W., Li, P., Zhou, H., Wang, Y., Zhang, Y., 2020. Molten salt induced nitrogen-doped biochar nanosheets as highly efficient peroxymonosulfate catalyst for organic pollutant degradation. Environ. Pollut. 260, 114053. https://10.1016/j.envpol.2020.114053.

Yang, J., Yang, H., Wang, S., Wang, K., Sun, Y., Yi, W., Yang, G., 2023. Importance of pyrolysis programs in enhancing the application of microalgae-derived biochar in microbial fuel cells. Fuel 333, 126244. https://doi.org/10.1016/j.fuel.2022.126244.

Yin, H., Lu, B., Xu, Y., Tang, D., Mao, X., Xiao, W., Wang, D., Alshawabkeh, A.N., 2014. Harvesting capacitive carbon by carbonization of waste biomass in molten salts. Environ. Sci. Technol. 48, 8101–8108. https://10.1021/es501739v.

Zeng, D., Dou, Y., Li, M., Zhou, M., Li, H., Jiang, K., Yang, F., Peng, J., 2018. Wool fiber-derived nitrogen-doped porous carbon prepared from molten salt carbonization method for supercapacitor application. J. Mater. Sci. 53, 8372–8384. https://10.1007/s10853-018-2035-8.

Zeng, K., Li, J., Xie, Y., Yang, H., Yang, X., Zhong, D., Zhen, W., Flamant, G., Chen, H., 2020. Molten salt pyrolysis of biomass: the mechanism of volatile reforming and pyrolysis. Energy 213, 118801. https://doi.org/10.1016/j.energy.2020.118801. Zeng, K., Yang, X., Xie, Y., Yang, H., Li, J., Zhong, D., Zuo, H., Nzihou, A., Zhu, Y., Chen, H., 2021. Molten salt pyrolysis of biomass: the evaluation of molten salt. Fuel 302, 121103. https://doi.org/10.1016/j.fuel.2021.121103.

Zhang, Y., Wang, J., Lv, P., Bie, N., Cao, P., Bai, Y., Song, X., Yu, G., 2022. Capture of released alkali metals and its simultaneously catalytic performance on secondary reactions of volatiles during biomass pyrolysis. Fuel 317, 123557. https://doi.org/10.1016/j.fuel.2022.123557.

Zhao, S.L., Liu, M., Zhao, L., Lu, J.H., 2017. Effects of organic and inorganic metal salts on thermogravimetric pyrolysis of biomass components. Kor. J. Chem. Eng. 34, 3077–3084. https://10.1007/s11814-017-0209-8.

Zhong, D., Chang, Z., Zeng, K., Li, J., Qiu, Y., Lu, Q., Flamant, G., Yang, H., Chen, H., 2023. Solar pyrolysis of biomass - part II: the physicochemical structure evolution of char. Fuel 333, 126474. https://doi.org/10.1016/j.fuel.2022.126474.

Zhou, Q., Ju, W., Liu, Y., Li, J., Zhang, Q., 2020. Effect of coexistence of defect and dopant on the quantum capacitance of graphene-based supercapacitors electrodes. Appl. Surf. Sci. 510, 145448. https://10.1016/j.apsusc.2020.145448.

Zhou, X., Wang, P., Zhang, Y., Wang, L., Zhang, L., Zhang, L., Xu, L., Liu, L., 2017. Biomass based nitrogen-doped structure-tunable versatile porous carbon materials. J. Mater. Chem. 5, 12958–12968. https://10.1039/C7TA02113E.

Zou, K., Guan, Z., Deng, Y., Chen, G., 2020. Nitrogen-rich porous carbon in ultra-high yield derived from activation of biomass waste by a novel eutectic salt for high performance Li-ion capacitors. Carbon 161, 25–35. https://10.1016/j.carbon.2020 .01.045.

Zuo, H., Zeng, K., Dian, Z., Li, J., Xu, H., Lu, Y., Lu, W., Zhou, H., Flamant, G., Yang, H., Chen, H., 2023. Design of a self-management solar pyrolysis packed-bed reactor by coupling thermal energy storage. Energy Fuel. 37, 2134–2148. https://10.1021/acs.energyfuels.2c03884.